Electronic Supplementary Material (ESI) for Nanoscale.

Rational design of metal organic frameworks-derived FeS_2 hollow nanocages@reduced graphene oxide for K-ion storage

Junpeng Xie,[a] Yongqian Zhu,[a] Ning Zhuang,[a] Hang Lei,[ab] Weiling Zhu[c], Yong Fu,[a] Muhammad Sufyan Javed,[a] Jinliang Li,*[a] Wenjie Mai*[a]

[a]*Siyuan Laboratory, Guangdong Provincial Engineering Technology Research Center of Vacuum Coating Technologies and New Energy Materials, Department of Physics, Jinan University, Guangzhou 510632, People's Republic of China. E-mail: lijinliang@email.jnu.edu.cn (Jinliang Li); wenjiemai@gmail.com (Wenjie Mai)*

[b]*Department of Chemistry, Jinan University, Guangzhou, Guangdong 510632, People's Republic of China.*

[c]*School of Science, Guangdong University of Petrochemical Technology, Maoming, Guangdong 525000, People's Republic of China.*

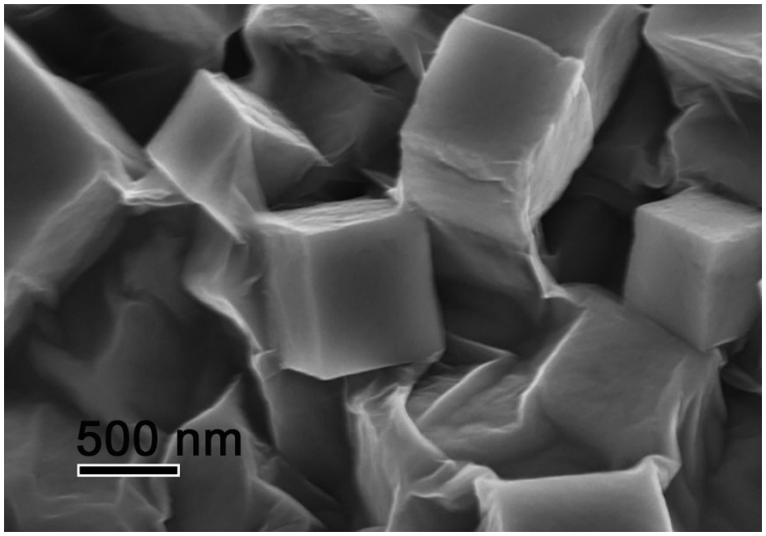

Figure S1 SEM image of PB@GO.

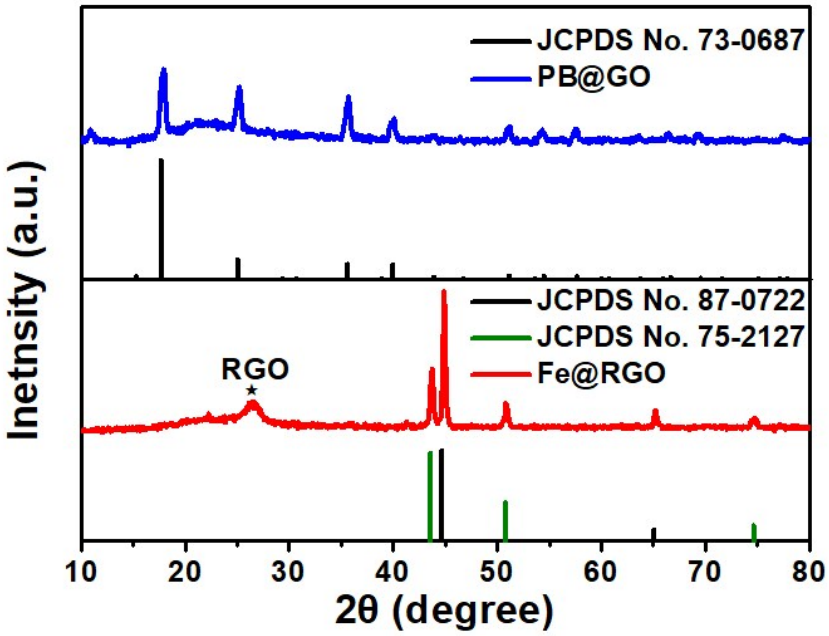

Figure S2 XRD patterns of PB@GO and Fe@RGO.

In the XRD pattern of Fe@RGO, a broad peak at 26° is attributed to (002) facets of RGO. Other diffraction peaks are assigned to Fe (JCPDS card No. 87-0722) and $FeN_{0.0324}$ (JCPDS card No. 75-2127). The result demonstrates that the RGO and Fe have been reduced after thermal treatment. The formation of $FeN_{0.0324}$ is mainly due to the existence of N element in PB. According to the previous reports, during annealing progress in N_2 or Ar atmosphere, transition metal anions will be reduced into pure transition metal, and CN- group linkers will form carbon compounds [1-3]. Furthermore, RGO is also an excellent reducing agent in high temperature, which is helpful for the reduction of Fe ion. Such phenomenon has been reported in other Co-Fe alloys, Ni-Fe alloys [1-3].

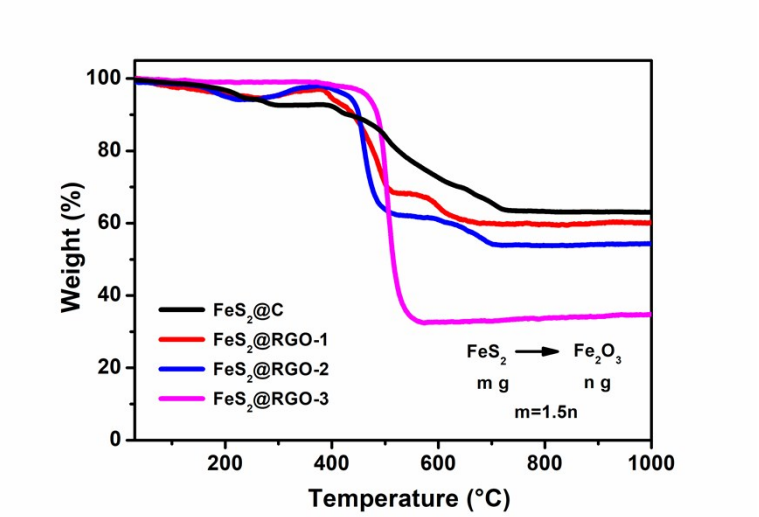

Figure S3 TGA curves of FeS_2@C, FeS_2@RGO-1, FeS_2@RGO-2 and FeS_2@RGO-3.

TGA curves were carried out to evaluate the carbon content in the composite, as shown in Fig. S3. After being heated to 700 °C, the weights of the samples become stable, and 63.4%, 59.0%, 53.8% and 32.9% of the original weight are left for the final products for FeS_2@C, FeS_2@RGO-1, FeS_2@RGO-2, FeS_2@RGO-3, respectively. Due to the oxidation of FeS_2 to Fe_2O_3 while the carbon to carbon dioxide, the carbon content of FeS_2@C, FeS_2@RGO-1, FeS_2@RGO-2, FeS_2@RGO-3 can be calculated, and corresponding values are 4.9%, 11.5%, 19.3% and 50.7%.

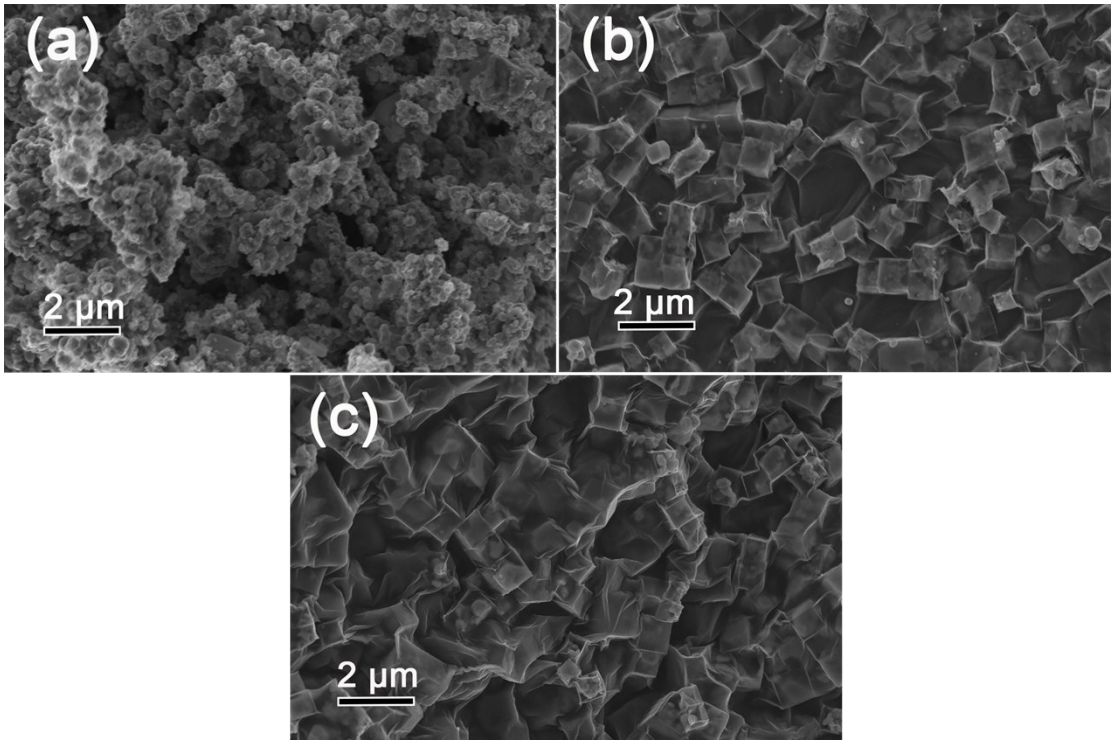

Figure S4 SEM images of (a) FeS_2@C, (b) FeS_2@RGO-1 and (c) FeS_2@RGO-3

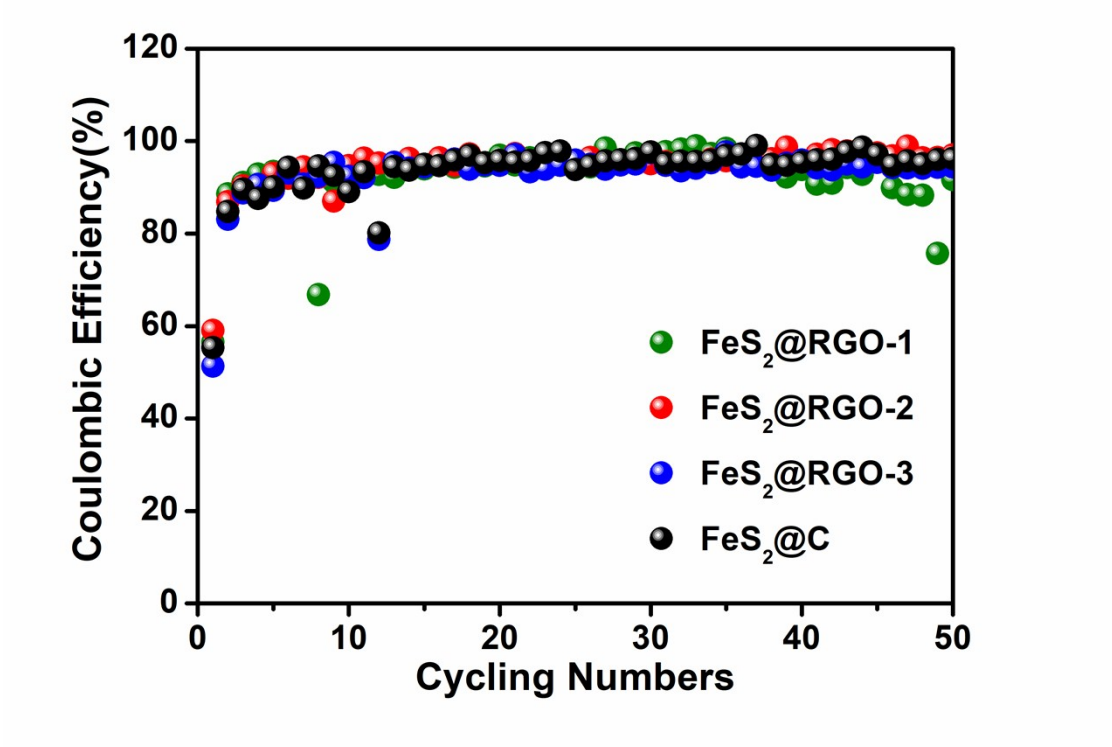

Figure. S5 Coulombic efficiencies of FeS_2@C, FeS_2@RGO-1, FeS_2@RGO-2 and FeS_2@RGO-3 at 50 mA g^{-1}.

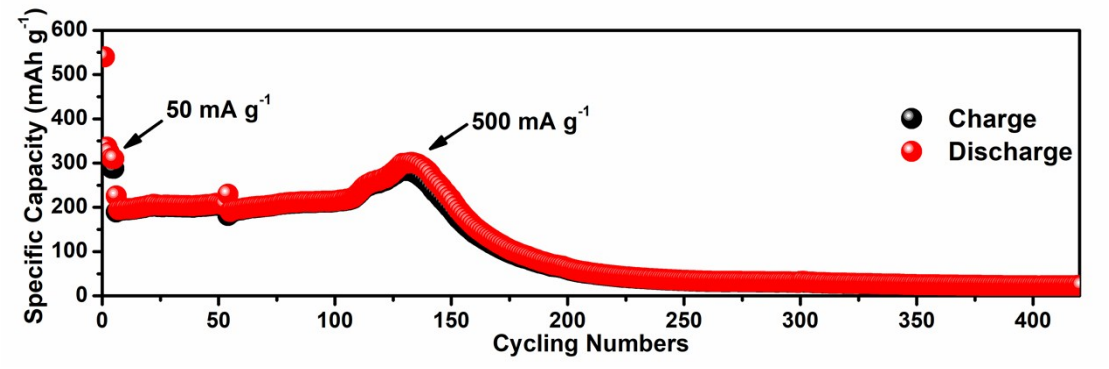

Figure S6 Long-term cycling performance of FeS_2@RGO-1 at 500 mA g^{-1}

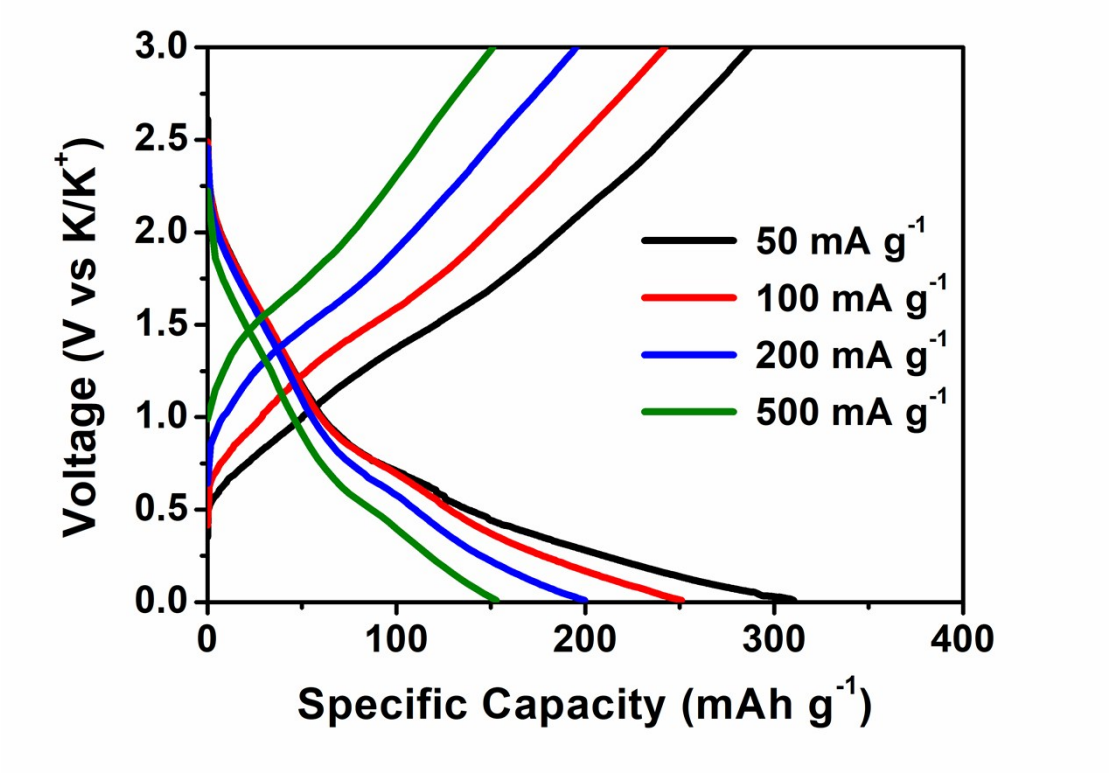

Figure S7 Galvanostatic charge-discharge curves of FeS_2@RGO-2 electrode at different current densities.

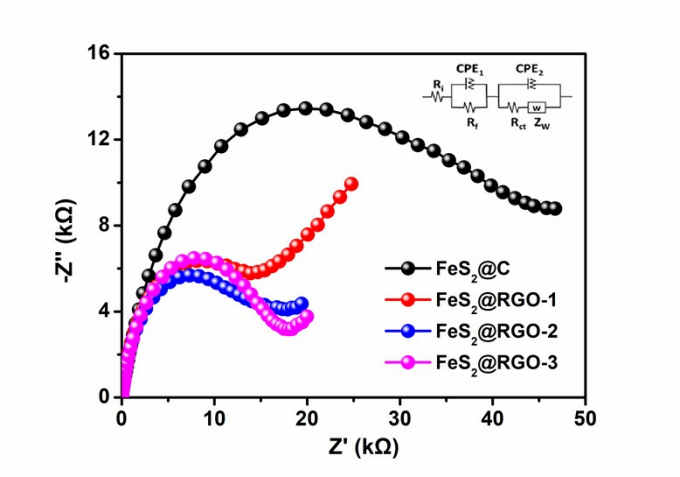

Figure S8 EIS of FeS_2@C, FeS_2@RGO-1, FeS_2@RGO-2 and FeS_2@RGO-3 after 10 cycles.

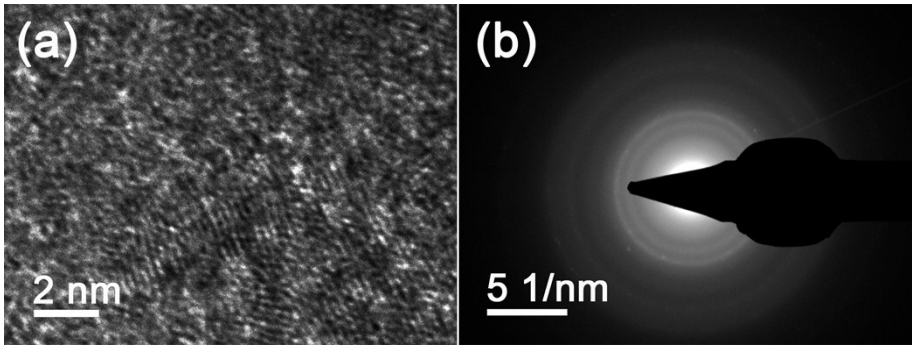

Figure S9 (a) HRTEM image of FeS_2@RGO-2 electrode when charging to 3.0 V and (b) the corresponding SAED image in the first cycle.

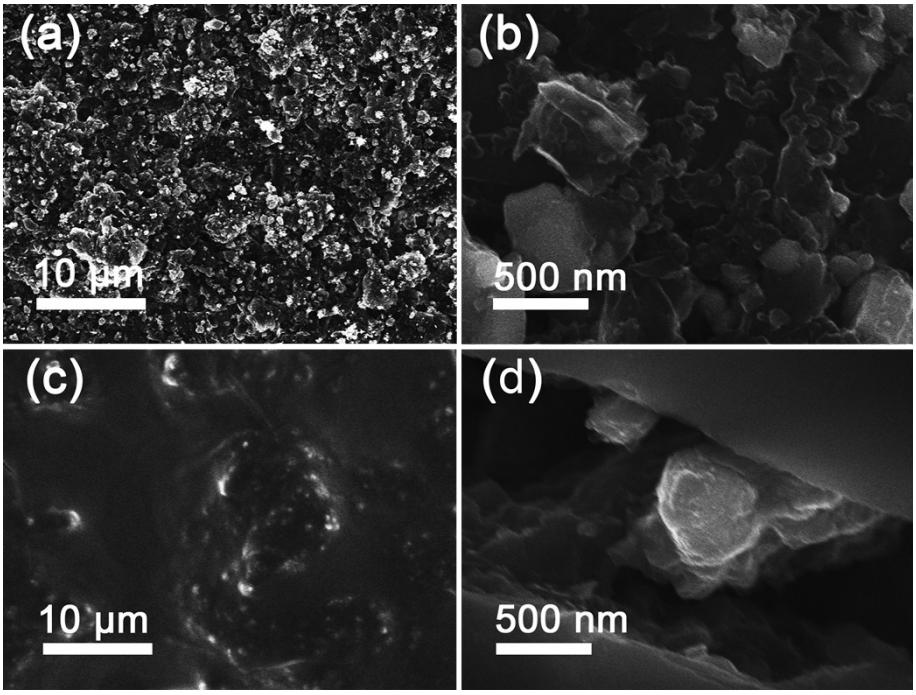

Figure S10 SEM images of FeS_2@RGO-2 electrodes. (a)-(b) before cycles, (c)-(d) after a number of cycles.

Reference

[1] P.W. Cai, S.Q. Ci, E.H. Zhang, P. Shao, C.S. Cao, Z.H. Wen, Electrochim. Acta, 220 (2016) 354-362.

[2] X.J. Zheng, J. Deng, N. Wang, D.H. Deng, W.H. Zhang, X.H. Bao, C. Li, Angew. Chem. Int. Edit., 53 (2014) 7023-7027.

[3] Z.H. Yang, H.L. Lv, R.B. Wu, Nano Res., 9 (2016) 3671-3682.